# Electron Scattering from the Deuteron and the Neutron-Proton Potential*

JOHN A. MCINTYRE† AND GEORGE R. BURLESON
*Department of Physics and High-Energy Physics Laboratory, Stanford University, Stanford, California*

(Received August 25, 1958)

Electron scattering by the deuteron has been studied experimentally at 400 and 500 Mev. The results of the scattering are compared with the scattering expected by three different static deuteron models. All three models satisfy the usual deuteron requirements such as binding energy, effective range, quadrupole moment, and percent $D$ state. Two of the models have Yukawa neutron-proton potentials; the third has a repulsive-core potential. The experimental results agree with the repulsive-core model and disagree with the Yukawa models. This result applies only to the triplet-$S$ neutron-proton potential.

## I. INTRODUCTION AND CONCLUSIONS

THE charge distribution of nuclei can be determined from the elastic scattering of high-energy electrons (~100 Mev) from nuclei.[1] With the exception of the deuteron, however, there is no reliable theoretical prediction of what the nuclear charge distribution should be like. In this respect, the deuteron is of particular interest since the nonrelativistic theory of the deuteron can be used to relate the charge distribution (wave function) determined by electron scattering to the kind of neutron-proton potential holding the deuteron together.

The usual theory of the deuteron is straightforward and rests on a very few fundamental assumptions.[2] The two main parameters of the theory are the deuteron binding energy and the effective range of the neutron-proton potential for the triplet $S$ state. The binding energy determines the behavior of the deuteron's wave function outside the nuclear potential and the effective range determines the range of the potential. Thus, the deuteron wave function is determined by these two parameters except for the region inside the potential well. Since the extent of the deuteron is 4.3 fermis [1 fermi(f) $\equiv 10^{-13}$ cm] whereas the effective range is only 1.70 f, it is seen that these two parameters determine quite well the deuteron wave function. These values also show that an electron scattering measurement to probe the deuteron charge inside the potential well will be difficult because only about $(1.70/4.3)^3 \sim 6\%$ of the deuteron charge is inside the well.

A considerable effort has been made in the past[2] to determine the deuteron wave function inside the nuclear potential. This amounts to determining, in addition to the effective range of the potential, a second "shape" parameter of the potential. The usual approach has been to make more precise measurements of the low-energy neutron-proton scattering[2] or of the photodisintegration of the deuteron.[3] In neither of these cases have sufficiently accurate data been obtainable, however. Another approach to the problem has been to study neutron-proton scattering at higher energies. More information about the neutron-proton potential is indeed gained, the most striking feature being that the potential has a repulsive core.[4] It would not be surprising, therefore, to find that the repulsive core also is present in the deuteron. A second line of investigation has led likewise to a repulsive core in the deuteron. Using the successful static meson-nucleon theory of Chew,[5] Gartenhaus calculated the form of the neutron-proton interaction[6]; his resulting potential had a repulsive core also. In conclusion then, low-energy data concerning the neutron-proton potential, yield only an effective range for the potential whereas higher energy data and a phenomenological meson theory indicate in addition that the potential should have a repulsive core.

Analysis of the electron-deuteron elastic scattering experiments is straightforward if relativistic effects in the bound two-nucleon system are neglected. Because of the small charge on the deuteron the first Born approximation can be used as Valk and Malenka have verified.[7] By using this Born approximation, Jankus[8] has calculated the elastic scattering from the deuteron including both the $S$- and $D$-state contributions and the scattering by the deuteron's magnetic moment (references to earlier calculations of the electron-deuteron scattering are given in Jankus' paper). It is important to note that Jankus' calculation is not a relativistic one in that the deuteron is treated as a static bound system. Thus, the deuteron wave function is considered as simply the product of Pauli two-component spinors for the neutron and proton wave functions, meson currents

* The research reported here was supported by the joint program of the Office of Naval Research and the U. S. Atomic Energy Commission, and by the U. S. Air Force through the Office of Scientific Research, Air Research and Development Command.

† Now at Yale University, New Haven, Connecticut.

[1] For a review of such investigations see R. Hofstadter, Revs. Modern Phys. **28**, 214 (1956).

[2] See, e.g., J. M. Blatt and V. F. Weisskopf, *Theoretical Nuclear Physics* (John Wiley and Sons, Inc., New York, 1952), Chap. 2.

[3] Barnes, Carver, Stafford, and Wilkinson, Phys. Rev. **86**, 359 (1952); D. H. Wilkinson, Phys. Rev. **86**, 373 (1952).

[4] R. Jastrow, Phys. Rev. **79**, 389 (1950); **81**, 165 (1951).

[5] G. F. Chew, Phys. Rev. **95**, 1669 (1954).

[6] S. Gartenhaus, Phys. Rev. **100**, 900 (1955).

[7] H. S. Valk and B. J. Malenka, Phys. Rev. **104**, 800 (1956). H. S. Valk [Nuovo cimento **6**, 173 (1957)] has also shown that inelastic effects such as virtual meson production contribute a negligible amount to the elastic scattering.

[8] V. Z. Jankus, Phys. Rev. **102**, 1586 (1956).

being neglected. Also, the neutron and proton are considered as point particles and the recoil of the deuteron is treated nonrelativistically.

The experimental results to be reported here are the fourth to be presented on electron-deuteron elastic scattering.[9–11] The previous results, however, did not have sufficient accuracy to distinguish between the different neutron-proton potentials. In this paper more accurate electron-deuteron scattering data are presented. These were obtained by modifications in the experimental apparatus as explained in Sec. II. The scattering angles were small enough so that the scattering from the $D$ state of the deuteron at all angles except one was less than 10% and the magnetic moment scattering was at all times negligible. The scattering data therefore determine the neutron-proton potential in the triplet $S$ state. The effect of the size of the proton in the deuteron[12] was eliminated experimentally by taking ratios between electron-proton scattering and the electron-deuteron scattering. The justification for this treatment of the proton size has been demonstrated by Blankenbecler[13] from relativistic field theory. His only assumption is that meson exchange currents can be neglected.

The experimental results obtained here are compared with the scattering calculated using three different deuteron models. The calculations are based on the Jankus[8] analysis of the deuteron scattering and have already been presented.[11] Two of the deuteron models have Yukawa potentials[14] and the other has a repulsive-core potential.[6] Comparison of the experimental data with the scattering curves for the three different static deuteron models analyzed shows agreement with the repulsive-core deuteron and disagreement with the two Yukawa deuterons. The evidence for this conclusion is presented (in Fig. 5) where the scatter of the experimental points indicates the reliability of the measurements.

It must be emphasized that this comparison is only for three specific static deuteron models. A systematic investigation of other deuteron models with various parameters must be carried out before the static repulsive-core deuteron model can be considered as being determined by the electron scattering data.

Finally, it is important to recall the limitation of the static deuteron calculation of Jankus. An investigation of the relativistic effects in the deuteron has been made by Blankenbecler[13] who considers a deuteron model composed of two spin-zero bosons. His calculation includes the effects of the contraction of the final-state wave function and the retardation of the binding potential. With a relativistic Yukawa model he finds that the corrections are negative and bring the scattering down to that expected from a static repulsive-core model at the $q$ values in this experiment (see Fig. 5). He finds no positive correction such as that calculated by Bernstein.[15]

In conclusion, it may be said then that an independent method for determining the triplet-$S$ potential between the neutron and the proton has been developed. This method gives results in agreement with other methods[2,3] for measuring the triplet-$S$ potential characteristics. In addition, however, the electron scattering method selects between potetials that have previously been indistinguishable. In particular, for the three potentials studied here, using the static deuteron calculation, the repulsive-core potential is to be preferred to the two Yukawa potentials.

## II. EXPERIMENTAL APPARATUS

The apparatus used in the electron scattering experiments at Stanford has been described previously.[1,10] In order to obtain more accurate data a number of modifications in the equipment were made. These modifications were the following: (1) installation of a nuclear-induction type probe to measure and regulate the magnetic field of the electron-beam deflecting magnet; (2) installation of a "beam sniffer" to insure that the electron beam was centered on the target; and (3) use of a liquid deuterium target.

The nuclear induction probe was built by Franz Bumiller. Its use permitted the magnetic field of the deflecting magnet to be kept fixed to better than 0.01%. Since the spread in energy of the electrons being studied in the experiment is approximately 1%, a 0.01% variation in their energy selection would have a negligible effect on the experimental results. On the other hand, the absolute energy of the electrons as determined by the integrated field of the deflecting magnet along the path of the electrons is known only to about 1%. This calibration was made by Panofsky, Woodward, and Yodh[16] who used a floating-wire technique and by Chambers and Hofstadter[17] who made a comparison with the calibration of the electron-scattering analyzing magnet. The absolute value of the electron beam energy, however, need not be known more accurately than this since ratios between the scattering by the proton and the deuteron are taken during the experiment and the strong energy-dependent part of the scattering cross section (Mott cross section) cancels out. It should be pointed out here that it is just as essential to stabilize the electron-scattering analyzing magnet spectrometer as it is to stabilize the electron-beam deflecting magnet. The analyzing-magnet stabilization was ac-

[9] J. A. McIntyre and R. Hofstadter, Phys. Rev. **98**, 158 (1955).
[10] J. A. McIntyre, Phys. Rev. **103**, 1464 (1956).
[11] J. A. McIntyre and S. Dhar, Phys. Rev. **106**, 1074 (1957).
[12] See Yennie, Lévy, and Ravenhall [Revs. Modern Phys. **29**, 144 (1957)] for a discussion of the effect of the finite size of the proton on the electron-deuteron scattering results.
[13] R. Blankenbecler, Phys. Rev. **111**, 1684 (1958).
[14] H. Feshbach and J. Schwinger, Phys. Rev. **84**, 194 (1951).
[15] J. Bernstein, Phys. Rev. **104**, 249 (1956).
[16] Panofsky, Woodward, and Yodh, Phys. Rev. **102**, 1396 (1956).
[17] E. E. Chambers and R. Hofstadter, Phys. Rev. **103**, 1454 (1956).

complished as before by using a magnet-current regulator. The magnet field was set by adjusting the magnet current as read on a potentiometer. Since the magnet current was being changed quite often during the course of the experiments a current drift of more than 0.02% was quickly noticed and corrected. Corrections of this magnitude did not occur very often. After most of the data had been taken a rotating coil type magnetic field probe was installed in the analyzing magnet by F. Bumiller and A. W. Knudsen. This probe measured the magnetic field to an accuracy of better than 0.01%. Spot checks between the magnet current reading and the rotating coil measurement of the field showed no significant discrepancy in the current measurement.

The "beam sniffer" consisted of a double-section ionization chamber. The collector plate for the first section was divided by a vertical cut into two halves whereas the collector plate for the second section was divided by a horizontal cut into two halves. The signals from these halves were then balanced against each other; by steering the electron beam a null reading could be obtained indicating that the beam was horizontally and vertically centered. The horizontal steering was achieved automatically by feeding the horizontal-balance error signal through an amplifier to the shunt of the second electron-beam deflecting magnet. The ionization chamber was placed about 10 ft beyond the target in order not to interfere with the analyzing magnet which could be swung around the target. The Faraday cup for measuring the electron beam was directly behind the ionization chamber. The chamber diameter was 18 in.; its active volume was connected to the atmosphere. The large size for the chamber was required because of the multiple scattering of the electron beam in the target 10 ft away and the fact that the Faraday cup was behind the ionization chamber. After most of the data were taken, a television camera[18] viewing a small scintillator next to the scattering chamber was installed. A continuous visual check of the beam was than possible although the scintillators became darkened after about 10 hr of operation. This television monitor however was not very sensitive in detecting whether the center of gravity of the $\frac{1}{2}$-in.-diam beam remained stationary. With the "sniffer" the beam center was held fixed to within $\pm\frac{1}{16}$ in. vertically, and accurately centered horizontally with a periodic excursion of $\pm\frac{1}{16}$ in. The vertical movement of the beam effectively changed the energy selection of the analyzing magnet (deflection vertical) by $\pm 0.04\%$. Since the elastically scattered electrons being detected by the magnet had an energy spread of approximately 1%, the $\pm 0.04\%$ variation was reasonably small although still possibly large enough to have some effect on the data taken. On the other hand, the periodic ($\sim$1/sec) variation of the horizontal beam position introduced by the feedback control would have a negligible effect on the angular measurement. For small scattering angles, where the effect is largest, the variation would amount to $\pm\frac{1}{16}/26 = \pm 0.14°$ in the determination of the angle of scattering (26 in. is the distance from the target to the analyzing-magnet entrance slit). Being periodic and small, this variation in the beam position can, therefore, be neglected.

The third modification in the apparatus was the construction and installation of a liquid deuterium target. The target assembly consisted of three reservoirs: a liquid nitrogen reservoir surrounding a liquid hydrogen reservoir which in turn surrounded the liquid deuterium reservoir. Hanging below these reservoirs and connected to the liquid deuterium reservoir was the liquid deuterium target. This target was $1\frac{1}{2}$ in. in diam and 8 in. long, the electron beam passing along the axis of the cylinder. The walls of the target were made of 0.004-in. stainless steel and the ends were hemispheres formed from 0.004-in. stainless steel sheet by a die press. The target was assembled by brazing in a hydrogen furnace and was tested to hold 200 psi pressure. The target was sufficiently long so that electrons scattered from the entrance or exit hemispherical ends could not pass through the analyzing magnet and into the counter. A copper, gold-plated heat shield with a 0.001-in. aluminum window surrounded the target. This heat shield was attached to the liquid nitrogen reservoir. To cut down radiation losses in the system all of the reservoirs were gold plated. This cost very little more than nickel plating and reduced the radiation losses by a considerable factor. Because of a limitation in space in the vertical direction, the filling tubes to the different reservoirs had to be limited to a few inches in length. The main heat leak to the liquid hydrogen reservoir was by conduction along the filling tubes; the main heat transfer to the liquid nitrogen reservoir was by radiation. The liquid nitrogen reservoir contained 14.5 l; the nitrogen evaporated in 14 hr. The liquid hydrogen reservoir contained 6.3 l; the hydrogen evaporated in 24 hr. The liquid deuterium reservoir and target contained 0.5 liter. The liquid deuterium was obtained by cooling and liquefying deuterium gas; about 45 min was required to fill the deuterium system with liquid. Most of the liquid hydrogen, however, was evaporated in this liquefying process and so the liquid hydrogen reservoir was always refilled after liquefying the deuterium. This hydrogen refilling operation took about 20 min. The liquid deuterium target was also used for liquid hydrogen by introducing hydrogen gas into the deuterium system at a few pounds psi positive pressure. The experimental advantage gained by using the liquid deuterium target was a counting rate 6 times higher than that attainable with the high-pressure (2000 psi) gas target, without introducing a background to be subtracted as with the solid ($CD_2$) target.

[18] General Precision Laboratory, Inc., Pleasantville, New York.

TABLE I. Deuteron properties of the three wave functions used in the electron scattering calculations.

| Neutron-proton potential | Binding energy (Mev) | Triplet effective range ($10^{-13}$ cm) | Quadrupole moment ($10^{-27}$ cm$^2$) | Percent $D$ state | Reference |
|---|---|---|---|---|---|
| Repulsive core | 2.226 | 1.75 | 2.90 | 6.8 | Gartenhaus[a] |
| Yukawa (1) | 2.23 | 1.71 | 2.74 | 4.2 | Feshbach and Schwinger[b] |
| Yukawa (2) | 2.23 | 1.68 | 2.77 | 2.8 | Feshbach and Schwinger[b] |
| Experimental | 2.226±0.003 | 1.70±0.03 | 2.74±0.02 | 4±2 | Blatt and Weisskopf[c] |

[a] See reference 6.
[b] See reference 14.
[c] See reference 2.

## III. THEORETICAL CONSIDERATIONS

The calculation of the electron-deuteron scattering cross sections for three static deuteron models has been described in some detail before.[11] As reviewed already in Sec. I the calculations are based on the work of Jankus.[8] Three different deuteron wave functions were substituted into the Jankus formula, the properties of these deuterons being summarized in Table I. Curves giving the contribution of the deuteron $S$ state, the deuteron $D$ state, and the deuteron magnetic moment to the scattering from these deuteron models may be found in reference 12 (Figs. 6, 7, and 8). These curves are for deuterons with point nucleons, the form factors plotted being denoted by $F_d$.

The effect of the proton size in the deuteron may be included in a simple manner.[12] If $F_d$ is the deuteron form factor for a deuteron containing point nucleons and $F_p$ is the form factor for the proton, then $F$, the form factor for the deuteron with a finite size proton, is given by the relation

$$F=F_d\times F_p. \tag{1}$$

Because scattering at relatively small angles is to be investigated in this paper, the charge distribution only in the proton needs to be considered. Thus, in the following, $F_p$ is to be considered as the form factor for the *charge distribution* of the proton. $F_p$ has been determined experimentally by Bumiller and Hofstadter.[19] The neutron *charge* extension, of course, has been assumed to be negligible in this discussion since the neutron charge is ignored in the Jankus calculation. Experimentally also, the neutron charge has been found to have a negligible geometric size.[20] Using Eq. (1) then, $F^2$ is found for the three deuteron models from the total $F_d^2$ values and an exponential proton with rms radius of[19] 0.80 f. The deuteron $F^2$ values so obtained are plotted in Fig. 1 along with the proton $F_p^2$ curve.

The experimental cross sections for the deuteron and proton scattering can be compared to these curves in the following manner. $F^2$ and $F_p^2$ are related to the experimental cross sections by the equations

$$F^2={}_d\sigma_{\text{exp}}/{}_d\sigma_{\text{Mott}}, \tag{2}$$

$$F_p^2={}_p\sigma_{\text{exp}}/{}_p\sigma_{\text{Ros}}. \tag{3}$$

${}_d\sigma_{\text{exp}}$ and ${}_p\sigma_{\text{exp}}$ are the electron-deuteron and electron-proton experimental scattering cross sections, respectively, and ${}_d\sigma_{\text{Mott}}$ is the Mott scattering cross section from a point deuteron[11] and ${}_p\sigma_{\text{Ros}}$ is the Rosenbluth[21] scattering cross section from a point proton. By combining Eqs. (2) and (3), $F^2$ may be expressed as

$$F^2=\left(\frac{{}_d\sigma_{\text{exp}}}{{}_p\sigma_{\text{exp}}}\right)\left(\frac{{}_p\sigma_{\text{Ros}}}{{}_d\sigma_{\text{Mott}}}\right)F_p^2. \tag{4}$$

Since ${}_p\sigma_{\text{Ros}}$ and ${}_d\sigma_{\text{Mott}}$ have been calculated and $F_p^2$ is known from the work of Bumiller and Hofstadter,[19] the experimental ratio in Eq. (4) is sufficient to determine the experimental values for $F^2$ which may then be compared to the calculated curves in Fig. 1. An absolute cross section is therefore not measured.

A special case for Eq. (4) occurs when ${}_d\sigma_{\text{exp}}$ and ${}_p\sigma_{\text{exp}}$ are measured at the same $q$ value, where $q$ is the momentum transferred in the scattering process in the center-of-momentum system. This follows from the fact that all of the $F$'s are functions of $q$ only. Thus, division of Eq. (4) by $F_p^2(q)$ yields [using Eq. (1)]

$$\frac{F^2(q)}{F_p^2(q)}=F_d^2(q)=\left(\frac{{}_d\sigma_{\text{exp}}}{{}_p\sigma_{\text{exp}}}\right)\left(\frac{{}_p\sigma_{\text{Ros}}}{{}_d\sigma_{\text{Mott}}}\right). \tag{5}$$

$F_d^2(q)$ is therefore determined independently of $F_p^2(q)$, i.e., independently of the proton size. Since $F_d^2$ is the quantity calculated from Jankus' formula, a comparison can be made directly between the deuteron model calculations and the experimental results without introducing the size of the proton. A number of deuteron/proton ratios were taken in this way (at the same $q$ values) so that the comparison made between the deuteron model calculations and the experimental data is independent of the proton size. However, for the sake of clearness in showing the method used and to demonstrate that the proton points obtained with the liquid target agree with the Bumiller-Hofstadter solid target data, the data have been plotted as shown in Fig. 1.

[19] F. Bumiller and R. Hofstadter, Bull. Am. Phys. Soc. Ser. II, 3, 50 (1958).

[20] Melkonian, Rustad, and Havens, Bull. Am. Phys. Soc. Ser. II, 1, 62 (1956); Hughes, Harvey, Goldberg, and Stafne, Phys. Rev. 90, 497 (1953). These experiments actually indicate only that the root-mean-square radius of the neutron is zero. L. I. Schiff [Revs. Modern Phys. 30, 462 (1958)] and A. Goldberg [Phys. Rev. 112, 618 (1958)] have investigated the possibility of a non-vanishing higher moment radius.

[21] M. N. Rosenbluth, Phys. Rev. 79, 615 (1950).

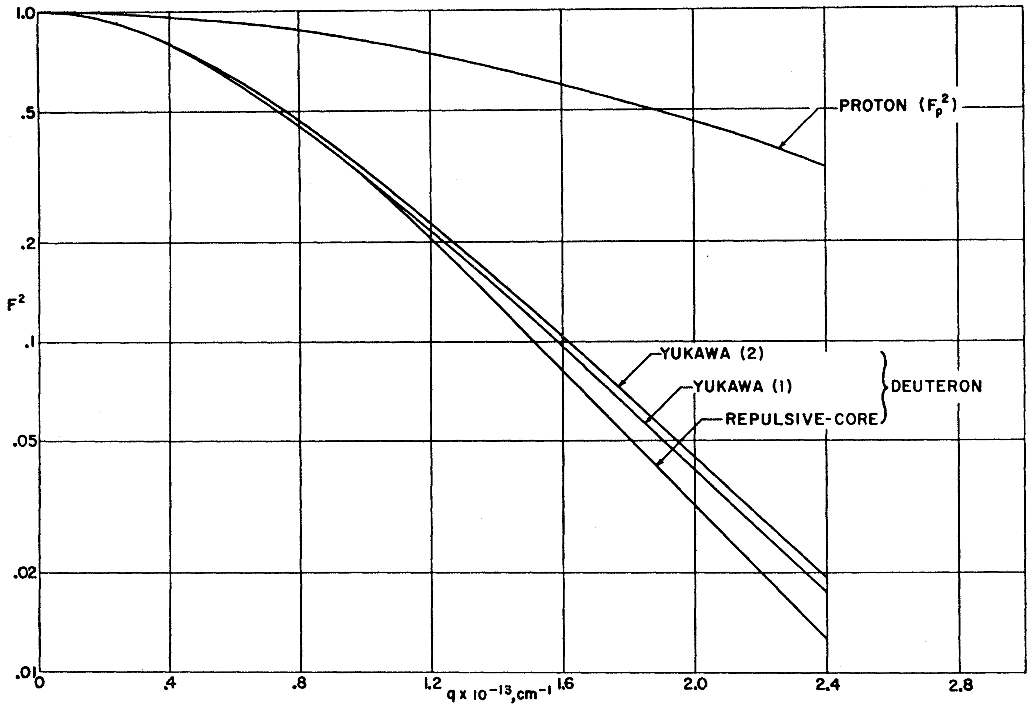


FIG. 1. $F^2$ values for the proton and for three static models for the deuteron. $F$, the deuteron form factor, includes the effect of the proton size. The proton form factor $F_p$ is that determined by electron-proton scattering[19] and is for a proton having an exponential charge distribution with rms radius of 0.80 f. $q$ is the momentum transfer in the center-of-momentum system.

## IV. EXPERIMENTAL DATA

As before,[11] scattered electrons were detected at various angles by transmission through the analyzing-magnet spectrometer. The detector of the scattered electrons was again a liquid Čerenkov counter. The pulse-height distribution from the counter is shown in Fig. 2. The setting of the discriminator is also shown; all pulses higher then the discriminator setting were counted.

A curve such as that shown in Fig. 3 of electrons counted *versus* analyzing-magnet current was obtained at each scattering angle, the area under the curve being a measure of the scattering cross section. Most of the curves taken had approximately 200 counts at the peak. No curve was taken with less than 100 counts in the peak. All curves had at least 12 points in the peak. At one angle a curve was repeated four times during a run; the areas under the four curves agreed with each other to within a few percent. However, a month later, the same curves were again repeated twice; the two repeat runs agreed with each other to within 3% but disagreed with the previous runs by 15%. Because of the occurrence of such effects, each run was normalized separately at one particular angle to either the $F_p^2$ curve (see Fig. 1) if a proton cross section were measured or to some previously measured deuteron point. Often various runs agreed within a few percent of each other; the discrepancy between runs was never more than the 15% value mentioned. The source of this variation between runs is not known. Using the previously described method of normalizing, the data were found to be consistent to an accuracy of about $\pm 5\%$.

Measurements were made at 400 and 500 Mev for scattering from both the deuteron and the proton. Most of the measurements were made with the liquid target. At the smaller angles two runs were made with gas targets and one with solid ($CD_2$ and $CH_2$) targets. The carbon subtraction for the $CD_2$ target was 30% at the peak, for the $CH_2$ target, 10%. A total of 38 elastic

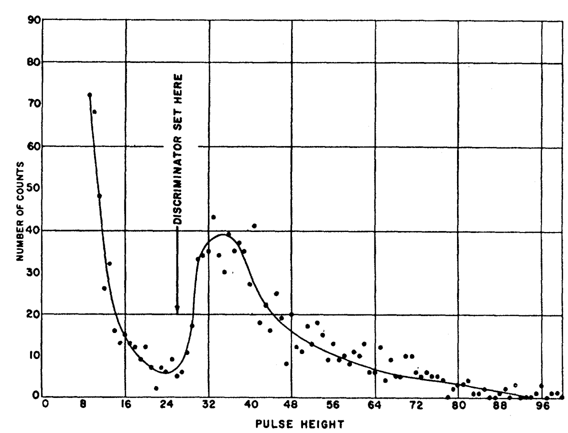


FIG. 2. Pulse-height distribution obtained with the Čerenkov counter. The setting of the discriminator is indicated by the arrow.

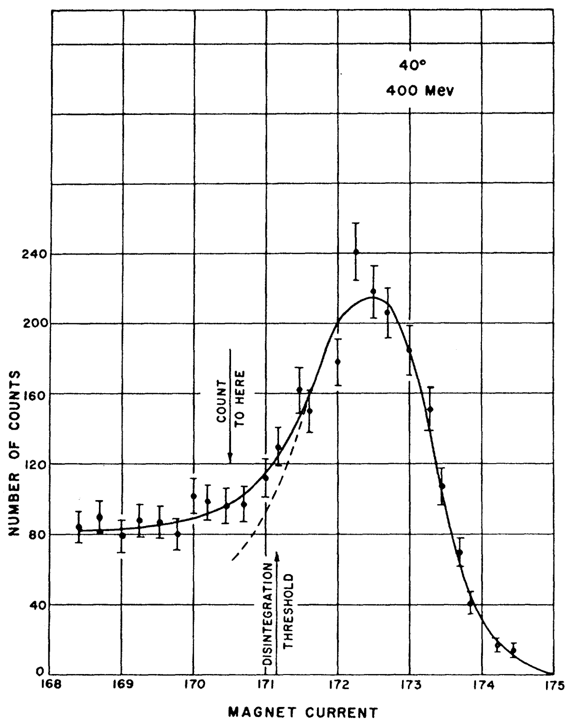


FIG. 3. The elastic scattering peak obtained at 40°, 400 Mev. The elastic scattering cross section is obtained from the number of counts in the dashed curve to the right of the upper arrow. The lower arrow indicates the deuteron disintegration threshold.

peaks were measured between 35° and 70°. One of the deuteron peaks obtained in one of the gas target runs was anomalously narrow and the cross section came out correspondingly small. This point was discarded on this basis. All of the other data for the various targets were consistent within the accuracy of the experiment, i.e., there were as large fluctuations among the liquid target data as occurred when comparing the liquid and the gas or the solid target data. The liquid target results were also checked by comparing the proton measurements with the electron-proton scattering results of Bumiller and Hofstadter[19] which had been taken with a solid target. Again a good check was obtained. By scattering from three kinds of targets a number of target correction factors could be verified. The target thickness of the solid target is determined by the target itself whereas in the liquid and gas targets the thickness is determined by one of the analyzing-magnet slits and the angle of scattering. Secondly, the target density could be verified: in the liquid, the deuterium density is 2.30 times that of the hydrogen whereas in the gas target the ratio is 2.00 if the pressures are the same. The agreement of the data therefore validated these corrections.

The cross section for the scattering at a given angle is proportional to the area under the elastic peak at that angle (see Fig. 3). Because of the indefiniteness of the boundary on the left side of the peak a consistent scheme for determining the left boundary was developed. It was assumed that the "true" shape of the scattering peak was given by the scattering peak obtained by electron-proton scattering. (The 45°, 500-Mev proton peak was used as the standard proton peak.) The electron-deuteron scattering peak in Fig. 3, on the other hand, is distorted on the left by inelastic scattering, i.e., scattering which has broken up the deuteron. The threshold for this scattering is only 2.2 Mev below the center of the elastic scattering peak as shown in the figure. Therefore, a peak having the "true" elastic shape (the proton peak shape) was fitted under the deuteron peak. The dashed curve in Fig. 3 is this fitted peak. The fitting was done by adjusting the width and the height of the standard proton peak until it fit the right side and the top of the deuteron peak. The left side of the proton peak was then considered to be the "true" left side of the elastic deuteron peak.

The area under the "true" deuteron peak in Fig. 3 was computed as follows. All of the counts represented by the experimental points were totaled from right to left until a point was reached which corresponded to an abscissa where the "true" (dashed) peak had dropped to 30% of its maximum value. From this total was then subtracted, for the few appropriate leftmost points, the difference in counts between the "true" (dashed) curve and the curve drawn through the experimental points. This left the number of counts represented by the "true" curve. This number was then multiplied by the appropriate magnetic field conversion factors, target geometrical factors, and the reciprocal of the beam magnitude to give a relative cross section for the angle of scattering investigated.

A small correction must be made for the fact that the proton peaks are in general wider than the deuteron peaks (because of the larger recoil of the proton in the scattering process). Thus more electrons that have lost a small fraction of their energy will be included by the wider peak. This effect has been calculated by Schwinger[22] and amounts to at most a percent or two for the variation in peak widths encountered in these experiments. Although the variation in the Schwinger correction can be neglected, the correction itself is such as to multiply the experimental values by 1.22, i.e., the elastic peaks accept only 82% of the elastic scattering.

The subtraction method just described for Fig. 3 gives an upper limit for the deuteron cross section, i.e., the dashed curve. This upper limit would not be the correct value however, if the inelastic scattering extended in a significant way under the elastic scattering peak. The "true" (dashed) elastic scattering peak in Fig. 3 would then have to be squeezed to the right and lowered. That the inelastic scattering could extend in a significant way under the elastic scattering peak seems possible because the threshold for the inelastic scattering

[22] J. Schwinger, Phys. Rev. 76, 790 (1949).

lies somewhat under the elastic peak (see Fig. 3) and the instrumental resolution would extend the inelastic scattering considerably to the right of the threshold.

In order to determine the importance of the inelastic scattering, the behavior of the scattering near the threshold must be known. This behavior has been calculated by Jankus[8] at 60° for 350-Mev scattered electrons. This angle and energy is not a great deal different from the experimental situation at 400 Mev. As a rough orientation then, the 60°, 350-Mev results will be used. These results (see Fig. 3 in reference 8) may be approximated rather well by the dotted (not dashed) curves shown in Fig. 4. The elastic scattering occurs essentially at one energy (the Schwinger correction will be ignored here) and has the cross section shown. The inelastic scattering rises abruptly at the threshold and remains constant in the region of interest near the elastic scattering peak. Its magnitude is considerably smaller than that of the elastic scattering. The dotted curves are then modified to include the effect of the instrumental broadening (see the dashed curves). The elastic scattering becomes a peak 1% wide to agree with the experimental widths of the deuteron peaks (a Gaussian line shape has been assumed for convenience) and the edge of the inelastic scattering is extended as shown assuming the same instrumental broadening. The sum of the two dashed curves then yields the total scattering, the solid curve. This solid curve represents the data taken in an electron-deuteron scattering experiment and is equivalent to the solid curve in Fig. 3. The left boundary of the curves in Fig. 4 is indicated by the arrow as in Fig. 3.

By taking areas to the right of the arrow in Fig. 4, the "true" (dashed) elastic scattering curve is found to enclose 3% less area then the total (solid) curve. Thus the inelastic scattering contribution to the total

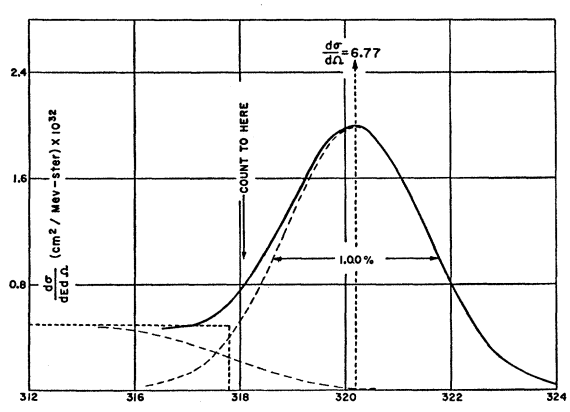


FIG. 4. Theoretical elastic and inelastic scattering cross sections at 60°, 350 Mev (indicated by dotted lines). Instrumental broadening similar to that obtained experimentally is then applied to the dotted curves and the dashed curves result. Addition of the two dashed curves gives the solid curve. The elastic scattering dashed curve and the solid curve are seen to be similar to the experimentally determined dashed and solid curves in Fig. 3.

peak would be only 3% if the total peak were used as the measure of the cross section. However, in Fig. 3, the total peak was not used; rather the "true" (dashed) peak was used which has 4% less area than the total peak. Therefore, the method used in calculating Fig. 3 seems to be a valid one to an accuracy of one percent.

This last remark must be qualified to some extent because the calculations for Fig. 4 are for 60° at 350 Mev whereas the experiment of Fig. 3 is for 40° at 400 Mev. Thus, a correction must be made for the difference in the scattering conditions. There are two ways for comparing, at different angles and energies, the inelastic scattering near the threshold with the elastic scattering: one by calculation, the other by experiment. Jankus[8] has calculated the two scatterings for two situations, namely 60° at 350 Mev as already mentioned and 70° at 190 Mev. The results are shown in Figs. 2 and 3 of reference 8. A ratio can now be taken between the inelastic scattering cross section near threshold and the elastic scattering cross section modified to take into account the fact that the elastic peak will have the same percentage width in each case. Surprisingly, this ratio between the inelastic and the elastic scattering cross sections is the same (within a few percent) for 70° and 190 Mev and 60° at 350 Mev. Since both the electron energy and the $q$ for the scattering are different for these two situations, this ratio will be assumed to be the same for all scattering situations in this energy and angle range and will be assumed to apply to the region of the experimental data also. The experimental results also confirm the method used in Fig. 3. If the ratio between the elastic scattering peak height and the height of the inelastic continuum as obtained experimentally is computed, this ratio is found to vary from 2.6 at 40° and 400 Mev to 1.8 at 60° and 500 Mev. Since the inelastic subtraction is only 3 to 4% at 40° and 400 Mev and since this subtraction is accounted for to within 1% by comparing Figs. 3 and 4, a variation of only 50% in the magnitude of the subtraction should not introduce an error of more than 1 or 2%.

It should be noted, however, that the ratio between the elastic peak and the inelastic continuum given by Jankus' calculations is 4.0 rather than 2.6 or less as found experimentally. Thus, there may be more inelastic scattering than has been assumed although this effect could hardly lower the deuteron cross sections more than a few percent. Further calculations of the inelastic scattering near threshold at the scattering angles and energies measured experimentally would certainly be of help here. Also, there may be experimental problems associated with the scattering of electrons from slits in the analyzing spectrometer which would broaden the elastic scattering peak. By taking the line shape to be that of the proton elastic scattering peak however, some of these effects should have been eliminated. The real solution to these problems would be to repeat the measurements with better resolution,

TABLE II. Summary of experimental results. (Normalized points are indicated by bold-faced type.) Normalization assumes an exponential proton with rms radius of 0.80 f.

| Run | Target | Energy (Mev) | Lab angle | $q$ ($f^{-1}$) | $F^2$ | $F_d^2 = F^2/F_p^2$ |
|---|---|---|---|---|---|---|
| I | Liquid $D_2$ | 404 | 40° | 1.36 | 0.136 | 0.198 |
| | | | 45° | 1.52 | 0.101 | 0.161 |
| | | | 50° | 1.66 | **0.0746**[a] | 0.129 |
| | | | 55° | 1.81 | 0.0546 | 0.104 |
| | | | 60° | 1.94 | 0.0435 | 0.0900 |
| | | | 70° | 2.19 | 0.0222 | 0.0550 |
| II | Liquid $D_2$ | 500 | 40° | 1.67 | **0.0746** | 0.130 |
| | | | 45° | 1.86 | 0.0431 | 0.0850 |
| | | | 50° | 2.04 | 0.0312 | 0.0696 |
| | | | 60° | 2.37 | 0.0141 | 0.0400 |
| III | Liquid $H_2$ | 404 | 40° | 1.33 | **0.726** | |
| | | | | | **0.724** | |
| | | 500 | 45° | 1.81 | **0.488** | |
| | | | | | **0.511** | |
| | Liquid $D_2$ | 404 | 50° | 1.66 | 0.0720 | 0.125 |
| | | | | | 0.0710 | 0.123 |
| | | 500 | 40° | 1.67 | 0.0760 | 0.132 |
| | | | | | 0.0794 | 0.138 |
| | | | 55° | 2.21 | 0.0196 | 0.0494 |
| IV | Liquid $H_2$ | 500 | 55° | 2.11 | 0.419 | |
| | Liquid $D_2$ | | | 2.21 | 0.0219 | 0.0551 |
| | Liquid $H_2$ | 400 | 70° | 2.05 | 0.430 | |
| | | | 45° | 1.46 | **0.670** | |
| | | | 40° | 1.32 | **0.681** | |
| | Liquid $D_2$ | | 45° | 1.50 | 0.0969 | 0.152 |
| | | | 40° | 1.35 | 0.146 | 0.211 |
| V | Gas $H_2$ | 400 | 35° | 1.18 | **0.738** | |
| | | | 40° | 1.32 | **0.720** | |
| | Gas $D_2$ | | 35° | 1.18 | 0.216 | 0.288 |
| VI | Solid $CH_2$ | 400 | 40° | 1.32 | **0.698** | |
| | Solid $CD_2$ | | | 1.35 | 0.160 | 0.231 |

[a] This measurement represents an average of four runs.

if the resulting loss in counting rate could be tolerated. A check along these lines was made by using $\frac{1}{4}\%$ instead of $\frac{1}{2}\%$ slits in the scattering apparatus at 40° and 404 Mev. The elastic scattering cross-section ratio between these two angles was the same within the usual accuracy for the two sets of slits. A more sensitive check could have been obtained if a proton point had also been taken. The proton-deuteron ratio was taken however for the solid target at 40° and 400 Mev. Because of the target geometry of the solid target the deuteron elastic scattering peak was narrow enough so that no inelastic scattering subtraction was required. Agreement was obtained with the liquid target results. (Because of the 30% carbon subtraction for the $CD_2$ target, the 10% agreement obtained between the liquid- and solid-target data can be considered satisfactory.) The deuteron point with the solid target was high which, if significant, would indicate that the inelastic contribution to the liquid target data has been overestimated.

A check on the calibration of the scattering angle was also made. Since the relative angular calibration had been checked before and is determined by a gear train, only one angle had to be calibrated. The zero-degree position was calibrated by setting the counter bias higher than for single pulses and by counting in the region of zero degrees. Because of pile-up in the counter, the most sensitive measurement proved to be a determination of the angle on each side of zero (±3°) where the counts disappeared. This angle was the same on both sides of zero to within 10′. The angular calibration was thus certainly accurate enough, particularly because the use of the deuteron-proton scattering ratios cancelled out the large angular dependent terms in the scattering cross sections.

The data obtained are listed in Table II and plotted in Fig. 5. Both $F^2$ and $F_d^2$ are listed for convenience. The curves of Fig. 1 are also shown in Fig. 5. Since $F^2$, the square of the form factor, is expected to be a function of $q$, the momentum transfer in the center-of-mass system, $F^2$ has been plotted against $q$. Thus, the 400- and 500-Mev data are intermingled in the figure. The 400- and 500-Mev data are distinguished in the figure by the symbols for the experimental points. Also, the gas target and solid target data are indicated. Some of the 400-Mev data were actually taken at 404 Mev and so some of the "400"-Mev data are found plotted at a slightly higher $q$.

The significance of the data in Fig. 5 depends on the method of normalization. This point can be best be discussed with reference to Table II. The data in Runs I–III were normalized with respect to the measurements of Run III. In that run, 40°, 404-Mev and 45°, 500-Mev proton scattering measurements were each made twice to give four values for $F^2$ as shown in Table II. These four values were normalized to best fit the proton curve in Fig. 5. With the proton points normalized, the deuteron measurements of Run III were determined. Inspection of Fig. 5 shows that the 500-Mev (×) proton points at $q=1.81\,\mathrm{f}^{-1}$ lie low whereas the 500-Mev (×) deuteron points at $q=1.67\,\mathrm{f}^{-1}$ lie high. If the proton points had been normalized to lie on the proton curve the deuteron points would have lain even higher. The opposite effect is apparent for the 404-Mev data. Here the proton points at $q=1.33\,\mathrm{f}^{-1}$ lie high. If they were lowered to the proton curve the deuteron points at $q=1.66\,\mathrm{f}^{-1}$ would be even lower. Thus, the method of normalization has minimized the discrepancy between the 404- and 500-Mev points. *This method of normalization has as its basis the $q$ dependence of the $F^2$ values.* The experiments then make use of this $q$ dependence rather than verifying the $q$ dependence.

The deuteron data taken in Runs I and II are then normalized to the deuteron data taken in Run III. Again, making the assumption that the $q$ dependence of $F^2$ is valid and that the discrepancies between the 404- and the 500-Mev data are statistical rather than real, the deuteron data for Runs I and II are normalized to the average of the 404- and 500-Mev data at $q=1.66\,\mathrm{f}^{-1}$ and $1.67\,\mathrm{f}^{-1}$, respectively ($F^2=0.0746$). With

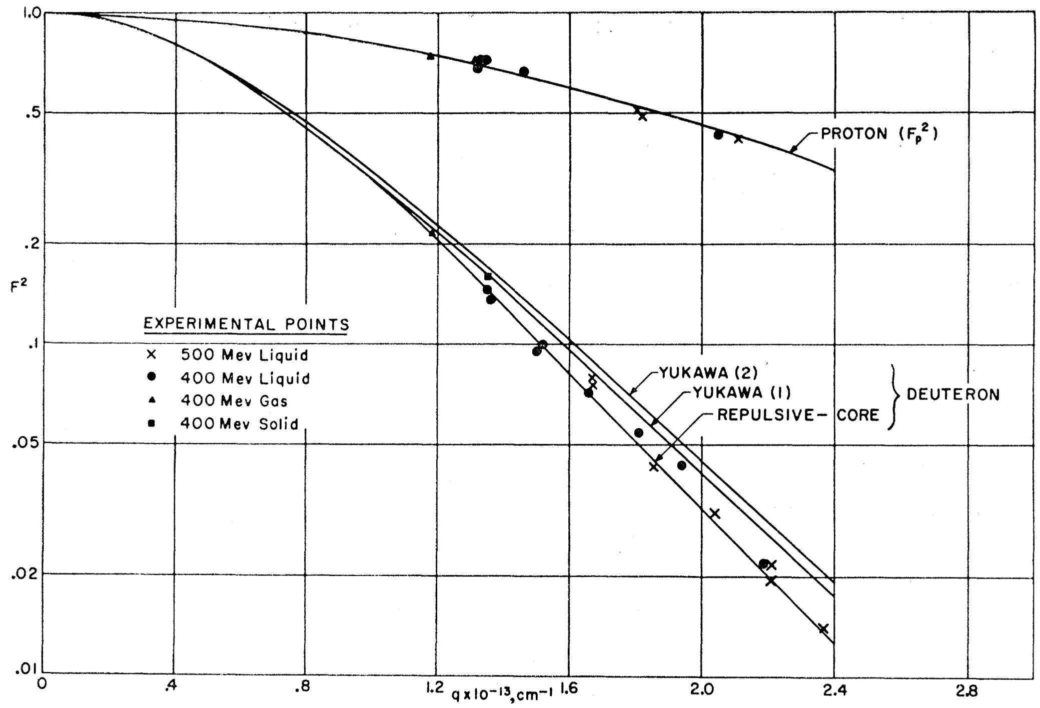


FIG. 5. Experimental results compared to the calculated scattering curves of Fig. 1.

this procedure the small-angle 404-Mev data ($q=1.36$ and 1.52) fit the theoretical curves. On the other hand, if the 500-Mev data had been ignored in the normalization procedure, these points would lie 8% lower. Within the accuracy of the experiment such a shift cannot be considered significant although the agreement between experiment and theory would look much poorer in Fig. 5. It should be pointed out here that no deuteron curve can be expected to lie below the repulsive-core curve in Fig. 5 at $q$ values smaller than $1.6\text{f}^{-1}$ because of effective-range considerations. This feature has been discussed previously.[11] Therefore, the points at small $q$ in Fig. 5 should not lie below the repulsive-core curve unless there is something seriously wrong with the method of analysis of the experiment.

Further inspection of Fig. 5 reveals the importance of the normalization of the deuteron points. With the scatter in the experimental points shown, a systematic shift vertically in the experimental points could easily lead to a fit to the wrong theoretical curve. Also the limitations in the experimental accuracy forbid distinguishing the curves except for the larger $q$ values measured. For these reasons a deuteron-proton scattering ratio was taken at 55°, 500 Mev. This measurement then checked the previous 55°, 500-Mev deuteron point and with it the entire normalization procedure. Also, the proton size correction would be cancelled out at this particular $q$ value ($q=2.21\text{f}^{-1}$) as explained in Sec. III. Finally, a check could be made of the shape of the proton curve in Fig. 5 by obtaining a point at large $q$. The result of this measurement was to obtain the proton point at $q=2.11\text{f}^{-1}$ and the upper of the two deuteron points at $q=2.21\text{f}^{-1}$; the higher deuteron value indicates that perhaps the previous 500-Mev points had been normalized a little low after all. However, considering the accuracy of the measurements the agreement can be considered good. Further measurements were made during this run at 400 Mev for the proton and the deuteron; all of the 400- and 500-Mev points for this run were normalized to the 40° and 45° proton points at 400 Mev. The closeness of the 55°, 500-Mev proton point ($q=2.11\text{f}^{-1}$) to the proton curve is a good check on the $q$ dependence of $F^2$ and the accuracy of the proton data in general.

Because of the importance of the normalization of the deuteron points and because of the fact that the liquid deuterium density was supposed to be 2.30 times rather than 2.00 times as dense as liquid hydrogen,[23] runs were made with gas and solid targets at small angles at 400 Mev. The gas point at $q=1.18\text{f}^{-1}$ and the solid point at $q=1.35\text{f}^{-1}$ show that the normalization with the liquid target is essentially correct. As mentioned before, the 30% carbon subtraction for the solid ($CD_2$) target makes this point more uncertain than the others.

Although the data all seem to be consistent and checks have been made for systematic errors, one somewhat disturbing feature still remains, namely, that the previous data taken with the gas target[11] tended to be somewhat higher than these data at the larger $q$ values. The reason for this discrepancy is not known.

[23] D. B. Chelton and D. B. Mann, University of California Radiation Laboratory Report UCRL-3421, 1956, (unpublished).

Certainly the effect is not a large one, the data in this report all lying within one probable error of the older data. Since the newer data are more consistent than the older data and have been checked in more ways, the discrepancy is believed to lie with the older data.

In conclusion, then, the data in Fig. 5 represent the electron elastic scattering from the deuteron. The accuracy of the points can be estimated by the scatter of the points. It is believed that there is no systematic error larger than the fluctuations in the data as shown in the figure.

## V. DISCUSSION OF RESULTS

The experimental results are compared to the three calculated deuteron curves in Fig. 5. These results indicate that the calculated scattering from the static model of the repulsive-core deuteron does agree with experiment while the two Yukawa-type deuteron models do not agree with the experiment. Reference to the calculated curves in reference 11 (Figs. 6, 7, and 8) shows that for the $q$ values investigated here experimentally, the $S$-state scattering accounts for more than 90% of the scattering cross section except for one $q$ value. Therefore, this conclusion applies only to the triplet-$S$ neutron-proton potential.

An interesting question then arises: can any other Yukawa-type deuteron model be made to fit the data? This can be answered only by a systematic investigation of the electron scattering to be expected for a wide range of Yukawa deuteron models which at the same time satisfy the necessary deuteron requirements (see Table I for these requirements). It may be of interest here to point out that an earlier calculation[10] showed that a square-well potential deuteron model scatters very much like a repulsive-core potential model over the range of $q$ values considered here.

It must be remembered that the preceding remarks are subject to the limitations in the calculational procedure which was used to compute the deuteron curves in Fig. 5. This procedure,[8] based on a static deuteron model, has been discussed in Sec. III and the limitations pointed out there and in Sec. I. A preliminary covariant calculation[13] of the electron-deuteron scattering indicates that all of the curves in Fig. 5 have to be lowered. This improved calculation may then alter the conclusion that the data favor a repulsive-core deuteron model.

## ACKNOWLEDGMENTS

It is a great pleasure to thank Professor Robert Hofstadter for his interest and encouragement in this work and for many helpful discussions. We are also indebted to Miss Monica Eder who assisted in taking data, Dr. Sobhana Dhar for help in constructing the liquid target, A. Marcum, E. Wright, and W. Ewings for design and construction of the liquid target, and C. Olson and L. Buss for design and construction of the "sniffer" electronics. Mr. R. Blankenbecler has kindly informed us of his calculations as they progressed and has helped us in interpreting the data. Discussions with Professor D. G. Ravenhall, Professor S. D. Drell, and Professor G. Breit are gratefully acknowledged. We also thank the many members of the electron scattering group who have contributed to the improvement and maintenance of the apparatus as well as the accelerator crew under Professor R. F. Mozley for operating the accelerator. Finally, we acknowledge with thanks a grant from Yale University which permitted J. A. McIntyre to complete the experimental work reported here.